Frontiers in Bioscience Landmark

Front. Biosci. (Landmark Ed) **2025**; 30(4): 33386
https://doi.org/10.31083/FBL33386

Original Research

Epigenetic Reprogramming by Decitabine in Retinoblastoma

Lisa Gherardini[1,*], Ankush Sharma[2,3], Monia Taranta[1], Caterina Cinti[4,*]

[1]Institute of Clinical Physiology, National Research Council of Italy, 53100 Siena, Italy
[2]Department of Cancer Immunology, Institute for Cancer Research, Oslo University Hospital, 0450 Oslo, Norway
[3]KG Jebsen Centre for B-cell malignancies, Institute of Clinical Medicine, University of Oslo, 0313 Oslo, Norway
[4]Institute for Organic Synthesis and Photoreactivity, National Research Council of Italy, 40129 Bologna, Italy
*Correspondence: lisa.gherardini@cnr.it (Lisa Gherardini); caterina.cinti@cnr.it (Caterina Cinti)

Academic Editor: Sung Eun Kim
Submitted: 28 November 2024 Revised: 21 February 2025 Accepted: 19 March 2025 Published: 25 April 2025

Abstract

Introduction: Retinoblastoma (Rb) is a rare cancer, yet it is the most common eye tumor in children. It can occur in either a familial or sporadic form, with the sporadic variant being more prevalent, though its downstream effects on epigenetic markers remain largely unclear. Currently, the treatment for retinoblastoma typically involves aggressive chemotherapy and surgical resection. The identification of specific epigenetic characteristics of non-hereditary (sporadic) Rb has led to the development of advanced, high-throughput methods to explore its epigenetic profile. Our previous research demonstrated that treatment with the demethylating agent 5-Aza-2′-deoxycytidine (decitabine; DAC) induced cell cycle arrest and apoptosis in a well-characterized retinoblastoma model (WERI-Rb-1). Our analysis of time-dependent gene expression in WERI-Rb-1 cells following DAC exposure has led to the development of testable hypotheses to further investigate the epigenetic impact on the initiation and progression of retinoblastoma tumors. **Methods**: Gene expression analysis of publicly available datasets from patients' primary tumors and normal retina have been compared with those found in WERI-Rb-1 cells to assess the relevance of DAC-driven genes as markers of primary retinoblastoma tumors. The effect of DAC treatment has been evaluated *in vivo*, both in subcutaneous xenografts and in orthotopic models. qPCR analysis of gene expression and Methylation-Specific PCR (MSP) was performed. **Results**: Our analysis of network maps for differentially expressed genes in primary tumors compared to DAC-driven genes identified 15 hub/driver genes that may play a pivotal role in the genesis and progression of retinoblastoma. DAC treatment induced significant tumor growth arrest *in vivo* in both subcutaneous and orthotopic xenograft retinoblastoma models. This was associated with changes in gene expression, either through the direct switching-on of epigenetically locked genes or through the indirect regulation of linked genes, suggesting the potential use of DAC as an epigenetic anti-cancer drug for the treatment of retinoblastoma patients. **Conclusion**: There is a pressing need to develop innovative treatments for retinoblastoma. Our research revealed that DAC can effectively suppress the growth and progression of retinoblastoma in *in vivo* models, offering a potential new therapeutic approach to battle this destructive disease. This discovery highlights the impact of this epigenetic therapy in reprogramming tumor dynamics, and thus its potential to preserve both the vision and lives of affected children.

Keywords: retinoblastoma; epigenetic reprogramming; cancer therapy; epigenetic therapy; DNA methyltransferase (DNMT) inhibitors

1. Introduction

Retinoblastoma (Rb) is a rare aggressive pediatric ocular cancer that represents the most common ocular tumor in children and its therapies and management often require intensive chemotherapy and sometimes surgery. Survivors are often challenged with long-term morbidity and poor quality of life related to their vision [1]. Retinoblastoma rapidly develops in immature retinal cells following biallelic inactivation of the *RB1* gene, resulting in the loss of RB1 function in more than 95% of cases [2]. Subsequent mutations and/or epigenetic modifications of other RB gene family members have been reported to play an important role in retinoblastoma tumorigenesis [3,4]. Given these observations, an integrated analysis of genomic and epigenetic modifications could help to identify new therapeutic approaches in attempts to spare children's sight and lives.

Epigenetic mechanisms can shape cell phenotype without modifying the DNA sequence and contribute to the regulation of tissue-specific gene expression. DNA methylation is one of the mechanisms for gene silencing, as dense methylation of DNA in promoter regions has been associated with transcriptional repression of chromatin [5]. This epigenetic phenomenon allows cells to respond to environmental changes in a transient manner, facilitating a functional reorganization of the genome while preserving DNA integrity. Recent advances in epigenomics have identified DNA methylation as one of the key mechanisms by which epigenetic regulation contributes to cancer progression, making it a target to interfere with cancer development and progression [6]. Thus, cancer therapy targeting epigenetic mechanisms holds significant promise, as it capitalizes on the reversible nature of epigenetically mediated alterations in gene expression.

Epigenetic-modulating drugs are already a reality in hematological malignancies and deserve adequate attention in solid tumors [7–9]. The DNA methyltransferase

inhibitor DAC (decitabine; 5-aza-2′-deoxycytidine) functions as a demethylating agent aimed at correcting epigenetic abnormalities. It facilitates the reactivation of silenced genes, particularly tumor suppressor genes, which play critical roles in regulating apoptosis and other key biological processes implicated in cancer development [10–13]. Recent studies have revealed that DNA methylation regulates multiple pathways in retinoblastoma [14–17]. However, the timeframe for demethylating agents to reverse the transcriptional inactivation of tumor suppressor genes remains poorly understood. In our previous study, we demonstrated the role of aberrant hypermethylation in primary sporadic retinoblastoma in patients [3], reinforcing the notion that treatment with demethylating agents could serve as an effective therapeutic strategy. Additionally, we have shown the efficacy of DAC in regulating gene expression in a retinoblastoma model (WERI-Rb-1) in a time-dependent manner [18]. We found that the antiproliferative effect of DAC is based on its influence on the expression of genes mainly involved in the regulatory pathways of TNF-, fatty acid synthase (FAS)-, p53-dependent apoptosis, and NF-κB pro-survival signaling. This generates a testable hypothesis regarding the impact of epigenetics on the genesis and progression of retinoblastoma tumors. To frame our previous results into a translational perspective, herein we investigated the relevance of DAC-driven genes as markers of retinoblastoma in primary tumors, and the possible use of DAC as a repurposed anti-cancer drug for the treatment of Rb patients.

2. Material and Methods

2.1 DAC-Driven Co-Regulated Genes in Patient-Derived Familial Retinoblastoma Samples and Interaction Network Maps

Publicly available Gene Expression Omnibus (GEO) database GSE59983 (https://www.ncbi.nlm.nih.gov/geo/) [19] from 76 retinoblastoma tissue samples, collected from patients who underwent primary enucleation without receiving previous treatment and profiled with Affymetrix human genome u133 plus 2.0 PM microarray, were analyzed using R package GEOquery [20]. Differentially expressed genes (DEGs) among primary tumors (N = 72) vs normal retinal (N = 4) were matched with previously obtained data of DAC-driven co-regulated genes from the WERI-Rb-1 cell line profiled using PIQORTM Cell Death Human Sense Microarrays [18].

GeneMania algorithm (http://www.genemania.org) was used to generate network maps of DEGs showing co-expression among connected genes. Functional enrichment analysis was obtained by the DAVID tool [21]. The resulting networks were exported to the Cytoscape platform (https://cytoscape.org/) for gene mapping and proper visualization of highlighted DEGs and their relationships. Gene ontology analysis for functional annotations of the differentially expressed genes was carried out using the Biological Networks Gene Ontology (BiNGO) and DAVID tools [21,22]. Cytoscape was also used to properly visualize the connections among genes and their biological functions.

2.2 DAC-Driven Hub Genes in Patient-Derived Sporadic Retinoblastoma Single-Cells

Public available single-cell transcriptome data from GEO database GSE142526 [23] of normal retina cells (human retinal organoids ORG_D104; ORG_D110 and retinospheres derived from human fetal retina RS_D134_pl_26FV) and from GEO database GSE196420 [24] of patient-derived non-familial retinoblastoma cells classified as E and D (**Supplementary Table 1**) according to the intraocular retinoblastoma classification (IIRC) (wRB6, RB006, RB010, RB015, RB016, RB018, RB020, and RB021) were also analyzed using the Seurat package [25] with a state-of-the-art pipeline previously utilized in [26,27]. Single-cell transcriptomes data were filtered based on defined criteria when genes expressed in cells $>$200 and number of RNA read counts were within 300 and 100,000 with mitochondrial percentage in cells $<$10. We also regressed cell cycle scores [28]. Clustering was performed using the Louvain algorithm, and Uniform Manifold Approximation and Projection (UMAP) visualization was generated [29]. The analyzed single-cell data (https://ankushs.shinyapps.io/Retinoblastoma_GSE196420/) is made available through the ShinyCell framework [27]. Differential expression of genes was computed using the R package GEOquery [20].

The Weighted Gene Co-expression Network Analysis package (WGCNA) [30,31] was used to reconstruct weighted gene co-expression networks for the differentially expressed genes in primary tumor and normal retinal cells. Edge weights, computed based on topology overlap measures, assigned co-expression correlation values between 0 and 1 to two connected genes (GEOquery). Subnetworks of 15 retinoblastoma hub genes were extracted from the co-expression networks of primary tumors using a threshold cutoff of 0.05 on edge weights among co-expressing genes. Cytoscape version 3.3 was used to visualize, and topological parameters were computed using Centiscape [27].

2.3 Cell Culture and Treatment

WERI-Rb-1 cells (ATCC, Manassas, VA, USA) were maintained in RPMI1640 medium (EuroClone, Milan, Italy) supplemented with 10% fetal bovine serum (EuroClone, Milan, Italy) and 2 mM L-glutamine, plus penicillin (100 U/mL) and streptomycin (100 mg/mL). The manufacture guarantee the cells are Mycoplasma Free and authenticated. Cells were split twice a week by resuspension in fresh media at a concentration of 3×10^5 cells/mL. For treatments, cells were seeded at a density of 2×10^5 cells/mL in six-well plates. After 24 h 2.5 µM 5-Aza-2′-deoxycytidine (Merck KGaA, Darmstadt, Germany) was added to the culture medium of the treated cells and main-

tained for up to 96 h. Control cells were treated in parallel with the vehicle.

2.4 Validation of 15 Hub Genes Expression by RT-qPCR Analysis

Total RNA was extracted from WERI-Rb-1 cells using the NucleoSpin RNA isolation kit (Macherey-Nagel, Duren, Germany) and from subcutaneous xenograft tumor samples using TRIzol reagent (Thermo Fisher Scientific, Waltham, MA, USA), according to the manufacturer's instructions. RNA concentration and purity were determined using a NanoDrop spectrophotometer (Thermo Fisher Scientific, Waltham, MA, USA). For each sample, 1 µg of total RNA was reverse transcribed using the Maxima H Minus First Strand cDNA Synthesis Kit (Thermo Fisher Scientific, Waltham, MA, USA). For the selected set of genes, qPCR validation was performed using the DyNAmo Flash SYBR Green qPCR Kit (Thermo Fisher Scientific, Waltham, MA, USA) with the PikoReal Real-Time PCR System (Thermo Fisher Scientific, Waltham, MA, USA). Primer specificity was checked using primer-BLAST (https://www.ncbi.nlm.nih.gov/tools/primer-blast) and confirmed by melting curve analysis. Primer pairs sequences are reported in **Supplementary Table 2a**. Amplification conditions were as follows: 7 minutes at 95 °C, followed by 40 cycles of 10 seconds at 95 °C, 20 seconds at 60 °C and 20 seconds at 72 °C. All samples were analyzed in triplicate. The relative expression of target genes was evaluated using the comparative cycle threshold method ($\Delta\Delta$CT), with β-actin (*ACTB*) used for normalization.

2.5 Methylation-Specific PCR (MSP)

DNA methylation in the promoter regions of selected genes (*CASP8*, *FAS*, *BIK*, *TP73*, *DAP3*, and *RRAD*) was analyzed by MSP, based on the differences between methylated and unmethylated DNA sequences, following sodium bisulfite treatment. Genomic DNA was extracted from WERI-Rb-1 cells and subjected to bisulfite modification using the EpiJET Bisulfite Conversion Kit (Thermo Fisher Scientific, Waltham, MA, USA). Modified DNA was then used for PCR reactions. Primer pairs for methylated (M) and un-methylated (U) sequences were designed to target CpG islands in promoter regions of the selected genes, using sequence data obtained from UCSC GENOME Browser (http://genome.ucsc.edu/cgi-bin/hgGateway). Primer specificity was validated through agarose gel electrophoresis of the PCR products, confirming the presence of a single band with the expected molecular weight. Detailed primer sequences are reported in **Supplementary Table 2b**.

2.6 Preclinical In Vivo Effect of DAC Epigenetic Treatment

Experiments were conducted on opportunistic pathogen-free the Naval Medical Research Institute (NMRI) male athymic BALB/c Nude mice, aged six to seven weeks (Harlan Laboratories, Udine, Italy), in accordance with EU Directive 2010/63/EU and the regulation of the Italian Ministry of Health. The mice were maintained on standard laboratory food and water that were available at all times, under a 12 h artificial light/dark cycle. After induction of deep anesthesia by inhalation of isoflurane in an induction chamber, the mice were euthanized using CO_2, as recommended by attachment IV Table 3 of EU Directive 2010/63/EU; 14G00036, GU Serie Generale n.61 del 14-03-2014, and Italian Ministry of Health. All the procedures were verified by the Ethics Committees of the Toscana Life Sciences and the Istituto Superiore di Sanità (ISS) on behalf of the Italian Minister of Health (Permit Number: # CNR-030314 and # CNR-101013) following ethical ICLAS and ARRIVE guidelines.

2.7 Retinoblastoma Xenograft Model

For the subcutaneous implants, animals were anesthetized using 2.5% isoflurane during the manipulation. WERI-Rb-1 cells, at a concentration of 3.6×10^7 in 100 µL 1× PBS, were injected subcutaneously in a 1:1 ratio with Matrigel TM basement membrane matrix (BD Biosciences, Franklin Lakes, NJ, USA) into the left flank of each mouse (total volume 200 µL). Once the grafts became palpable, their volume was measured using a digital caliper (length $\times$ width^2/2), and animals were assigned to experimental groups through minimization following the ARRIVE guidelines [32] to start the treatments. Tumor volume (mm^3) was measured biweekly and confirmed by ultrasound imaging (VisualSonics VEVO 2100, Fujifilm Sonosite Inc., Bothell, WA, USA) in the last session of measurement.

2.8 Retinoblastoma Orthotopic Model

The orthotopic retinoblastoma model was established unilaterally in one eye by injecting 1×10^4 WERI-Rb-1 cells in 10 µL of PBS. Briefly, under an operating microscope and using a Hamilton syringe 32 gauge, (cod: 12301828 Fisher Scientific Italia, Segrate (MI), Italy) the right eye globe of anesthetized animals was punctured laterally, through the conjunctiva and sclera, to access the vitreous cavity. Ultrasound Imaging (VisualSonics VEVO 2100, Fujifilm Sonosite Inc., Bothell, WA, USA) was used to establish the tumor appearance. Treatment began before visible leukocoria (white reflex in the eye pupil) appeared in the affected eye. Volume measurements were performed for group assignment (baseline) and then once a week to minimize animal distress due to repeated anesthesia.

2.9 In Vivo Drug Administration and Tissue Retention

In both experimental settings (xenograft and orthotopic retinoblastoma models), the treated groups received biweekly I.V. injections of 300 µL of 75 µg DAC in PBS buffer (meaning a therapeutic dose of 2.5 mg/kg), while the control groups received the vehicle. At the end of each

measurement and treatment session, the animals were monitored for signs of distress and allowed to recover in the original cages. After 3 weeks of treatment, the mice were euthanized via CO_2 inhalation. No signs of distress were observed [32] and no animals died during the treatments. Resected tumor masses from subcutaneous xenografts were processed using TRIzol reagent (Thermo Fisher Scientific, Waltham, MA, USA) and stored at –20 °C for further qPCR analysis.

2.10 Ultrasound Live Imaging in Orthotopic Mouse Model

The VisualSonics Vevo 2100 imaging system (VisualSonics VEVO 2100, Fujifilm Sonosite Inc., Bothell, WA, USA) was utilized to measure retinoblastoma growth within the eye. Animals were anesthetized with 5% isoflurane at an oxygen flow rate of 2 L/min (maintained at 2.5% isoflurane at an oxygen flow rate of 2 L/min) and placed on a warming pad in a prone position to facilitate signal acquisition while monitoring temperature, respiratory and heart rate. B-mode images were acquired using the MS-550 Blue transducer (central frequency, 40 MHz) connected to a 3-dimensional motor collecting frames 0.5 mm apart in the eye region. In the orthotopic model, for off-line analysis, a field of interest (FOI) outlining the tumor boundaries in the eye was drawn for reconstruction in 3D B-mode. These results were normalized to baseline (volume at tumor appearance) and expressed as fold increase (V = Vtx/Vt0) $\pm$ sem.

2.11 Statistical Analysis

For the *in vitro* experiments the results represent the mean $\pm$ SEM of at least three independent experiments. Two-Way ANOVA was used to evaluate the impact of decitabine on cell cycle phases at the different time points (24, 48, and 72 h). Similarly, Two-Way ANOVA was used to describe the significance of the longitudinal effect of the treatment on the number of apoptotic cells (mean $\pm$ SEM). For qPCR data, ΔCt values were subjected to a one-sample *t*-test and are shown as mean $\pm$ SD. To analyze the effect of time and treatment (DAC) on the tumor growth respectively in subcutaneous and orthotopic Rb xenograft models we applied two-way ANOVA repeated measure analysis for both time and treatment parameters (recommended Sidak analysis; GraphPad-Prism 7.0e, GraphPad Software, Inc., Boston, MA, USA). Results are expressed as mean $\pm$ SEM.

3. Results

3.1 DAC-Driven Genes as Markers of Primary Human Retinoblastoma Tumors

To assess whether the co-regulated clusters of genes (**Supplementary Fig. 1**), previously identified in DAC-treated WERI-Rb-1 cells [18], could represent candidate markers and potential therapeutic targets of DAC for primary retinoblastoma tumors, we performed a comparative analysis of differentially expressed genes (DEGs) in primary tumors versus WERI-Rb-1 cells. Publicly available transcriptome datasets from patient-derived samples and low-passage patient-derived single-cells were analyzed [19,23,24].

Table 1 reports the most significant time-related DEGs in WERI-Rb-1 cells after exposure to DAC within the co-regulated genes clusters, previously identified through the analysis of PIQORTM Cell Death Human Sense Microarrays data [18].

A strong down-regulation of pro-survival signals is observed at a short latency (48 h) following DAC treatment. These signals include several pro-mitogenic mediator surface molecules (*RASL10B*, *TOLLIP*, and *TRAF2*), intracellular MAPK members (*MAPK8IP1*, *MAPK8IP2*, *MAPK12*, *IRAK1*, *IKKB*, and *NFKB3*), and intracellular anti-apoptotic mediators (*BCL2L1*, *MKL1*, *JUNB*, *BIRC5*, and *FOS*). Conversely, genes playing a role in cell cycle arrest, like *PPP1R15A*, *STAT1*, and *CDKN1A*, are overexpressed starting 48 h after DAC treatment. Furthermore, significant activation of pathways associated with pro-apoptotic signals becomes evident 72 h after DAC treatment. In particular, a significant over-expression of several apoptotic mediator surface antigens, such as *FAS*, *DAP3*, and *TRAMP* receptors as well as intracellular pro-apoptotic members like *PSMD2*, *ALG2*, and *GAPD*, along with members of the caspases cascade (e.g., *CASP8*, *CASP3*, and *CASP6*) is observed. Concurrently, the p53-dependent pathway, which includes *CDKN1A*, *CDC10*, *PIG8*, and *BAX*, is activated, indicating a potential triggering of cytochrome C release in combination with other mechanisms (e.g., p73-dependent *BCL2L1* repression via *BIK*). The simultaneous down- and up-regulation of all these pathways may explain the effective anti-cancer activity of DAC in WERI-Rb-1 cells.

Interestingly, a notable overexpression of genes associated with DNA repair signaling, such as *PARP1* and *LIG4* (DNA LIGASE IV), along with tissue-specific genes like *PPM1D* (a photoreceptor-related gene) and *AKAP12* (a gene related to hemato-retinal barrier), both involved in visual signals [19,33], was observed at a later time point (96 h), suggesting a possible reprogramming action of DAC in the surviving cells. To investigate the potential of these DAC-driven genes as markers of primary retinoblastoma tumors, a gene expression profile analysis was performed comparing whole transcriptome microarray datasets of tumor cone photoreceptor lineages vs normal retinal cells. Both cell types were derived from frozen tissue samples collected after primary enucleation in patients with familial retinoblastoma [19]. The analysis identified 463 up-regulated genes, with a Log fold change greater than 2, and 282 down-regulated genes, with a Log FC $\leq$–2 (see **Supplementary Table 3**).

Among the 463 up-regulated genes, 136 are mainly linked to biological processes involved in cell proliferation, including *RASL10B*, *TRAF2*, *RELA*, *FOS*, *BCL2L1*,

Table 1. List of the most representative DAC co-regulated genes identified by cDNA microarray hierarchical clustering analysis.

Cluster	Name	48 h	72 h	96 h
0	**JUNB** (AP-1) JunB proto-oncogene, AP-1 transcription factor subunit	–3.32	–1.20	0
0	**FOS** (AP-1; C-FOS; p55) Fos proto-oncogene, AP-1 transcription factor subunit	–2.18	0	0
0	**MAPK8IP2** (IB2; JIP2; PRKM8IPL) C-JUN amino-terminal mitogen activated protein kinase 8-interacting protein 2	–2.25	–1.18	0
0	**MAPK8IP1** (B1; JIP1; JIP-1; PRKM8IP) C-JUN amino-terminal mitogen-activated protein kinase 8-Interacting protein 1	–2.89	–1.00	0
0	**RASL10B** (RRP17; VTS58635) RAS-like family 10, member B	–2.32	–1.50	0
0	**MAPK12** (ERK3; ERK6; SAPK3; PRKM12; SAPK3; P38GAMMA) mitogen-activated protein kinase 12	–2.73	–1.00	0
0	**MRTFA** (MAL; MKL; BSAC; MKL1; MRTF-A) Megakaryoblastic leukemia-1 protein	–2.32	–1.50	0
0	**RELA** (NFKB3) RELA proto-oncogene, NF-κB subunit	–2.89	–1.00	0
0	**BCL2L1** (BCL-XL) apoptosis regulator BCL2 Like 1	–2.52	–1.82	0
0	**TRAF2** (MGC:45012, RNF117, TRAP) TNF receptor associated factor 2	–2.73	–1.77	0
0	**TOLLIP** (IL-1RAcPIP) Toll interacting protein	–2.65	–1.00	0
0	**IKBKG** (IKKG; IP; FP3; NEMO) Inhibitor of nuclear factor kappa B kinase regulatory subunit gamma	–2.69	–1.00	0
0	**HSF1** (HSTF1) Heat-shock transcription factor	–2.00	–1.00	0
0	**IRAK1** Interleukin-1 receptor-associated kinase 1	–2.74	–1.18	0
0	**TICAM1** (TRIF, IIAE6; MyD88-3) TIR domain containing adaptor molecule 1	–1.98	–1.00	0
0	**TRIM28** (KAP1 PPP1R157, RNF96, TF1B, TIF1B, TIF1beta) tripartite motif containing 28	–2.64	–1.00	0
0	**DAXX** (BING2, DAP6, EAP1, SMIM40) FAS death domain-associated protein	–2.00	–1.00	0
0	**BIRC5** (API4; EPR-1; SURVIVIN) baculoviral IAP repeat containing 5	–2.00	–1.00	0
1	**CASP8** (CAP4; MACH; MCH5; FLICE; ALPS2B; Casp-8) caspase	1.00	2.90	0
2	**BAX** (BCL2L4) BCL2 associated X, apoptosis regulator	0	0	2.15
2	**CDKN1A** (P21; CIP1; SDI1; WAF1; CAP20; CDKN1; MDA-6; p21CIP1) Cyclin-dependent kinase inhibitor 1A	0	1.00	2.05
2	**MAPK6** (ERK3, HsT17250, PRKM6, p97MAPK) Mitogen-activated protein kinase 6	0	0	1.85
2	**PPP1R15A** (GADD34) Protein phosphatase 1 regulatory subunit 15A	1.00	0	1.75
2	**DAP3** (DKFZp686G12159, MGC126058, MGC126059, MRP-S29, MRPS29, bMRP-10) Mitochondrial ribosome small 28s subunit	0	0	2.08
2	**GAPDH** (G3PD, GAPD, HEL-S-162eP) Glyceraldehyde-3-phosphate dehydrogenase	0	0	2.00
2	**SEPT7** (CDC10; CDC3; Nbla02942) Septin7	1.00	1.00	1.77
2	**TNFRSF25** (APO-3, DDR3, DR3, GEF720, LARD, PLEKHG5, TNFRSF12, TR3, TRAMP, WSL-1, WSL-LR) TNF receptor superfamily member 25 apoptosis mediator	1.00	1.00	1.74
2	**ALG2** (PDCD6; CDG1I; CDGIi; CMS14; CMSTA3; NET38; hALPG2) Programed cell death 6	1.00	0	1.75
2	**TP53** (P53; BCC7; LFS1; BMFS5) Tumor protein p53	0	1.00	1.95
2	**TP73** (P73; CILD47) Tumor protein p73	0	1.00	1.95
2	**CASP6** (MCH2; CSP-6; caspase-6) Caspase 6	0	0	2.15
2	**STAT1** (CANDF7, IMD31A, IMD31B, IMD31C, ISGF-3, STAT91) Signal transducer and activator of transcription 1	1.00	0	1.57
2	**GPS1** (CSN1; SGN1; COPS1) G protein pathway suppressor 1	0	0	1.77

Table 1. Continued.

Cluster	Name	48 h	72 h	96 h
3	**CASP3** (CPP32; SCA-1; CPP32B) Caspase 3	0	1.00	2.86
3	**RERG** (MGC15754) RAS like estrogen regulated growth inhibitor	0	1.00	2.82
3	**PARP1** (PARP; PARS; PPOL; ADPRT; ARTD1; ADPRT1; ADPRT 1; pADPRT1; Poly-PARP) poly [ADP-ribose] polymerase-1	0	0	2.62
3	**LIG4** (LIG4S) DNA ligase 4	0	0	2.67
3	**EI24** (EPG4; PIG8; TP53I8) EI24 autophagy associated transmembrane protein	0	0	2.74
3	**STAMBP** (AMSH; MICCAP) STAM binding protein	0	0	2.76
3	**RRAD** (RAD; RAD1; REM3) Ras related glycolysis inhibitor and calcium channel regulator	0	1.00	3.23
3	**PQBP1** (SHS; MRX55; MRXS3; MRXS8; NPW38; RENS1) Polyglutamine binding protein 1	0	0	4.80
3	**PPM1D** (JDVS; WIP1; IDDGIP; PP2C-DELTA) protein phosphatase Mg^{2+}/Mn^{2+} dependent 1D	0	1.00	3.49
3	**CCNG2** Cyclin G2	1.00	1.00	3.53
3	**AKAP12** (SSECKS; AKAP250) A-kinase anchoring protein 12	1.00	1.00	2.48
3	**PSMD2** (S2; P97; RPN1; TRAP2) Proteasome 26S subunit ubiquitin receptor	1.00	1.00	2.70
3	**FAS** (APT1; CD95; FAS1; APO-1; FASTM; ALPS1A; TNFRS6) Fas cell surface death receptor	1.00	2.00	2.80
3	**BIK** (BP4; NBK; BIP1) BCL-2 interacting killer	2.22	2.86	1.45

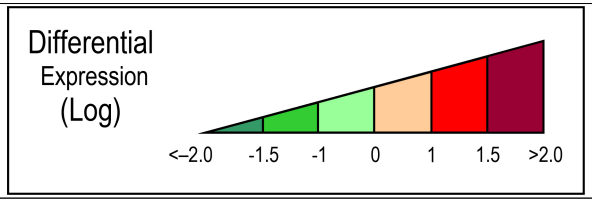

For each gene the Log fold change expression value is reported after 48 h, 72 h, and 96 h of DAC treatment. Cluster 0 includes the genes whose expression is downregulated earliest at 48 and 72 h after DAC treatment, with logarithmic values ranging from –1.5 to –3.30. Clusters 1, 2, and 3 include the genes whose expression is upregulated starting at the earliest stage (48 h) and increasing over time, reaching a maximum at 96 h, with logarithmic expression values ranging from +1 to +4.8. The color gradation of each square (green down-regulated and red up-regulated genes) represents the measured differential expression value referred to the logarithmic scale (Log). DAC, 5-Aza-2′-deoxycytidine (decitabine).

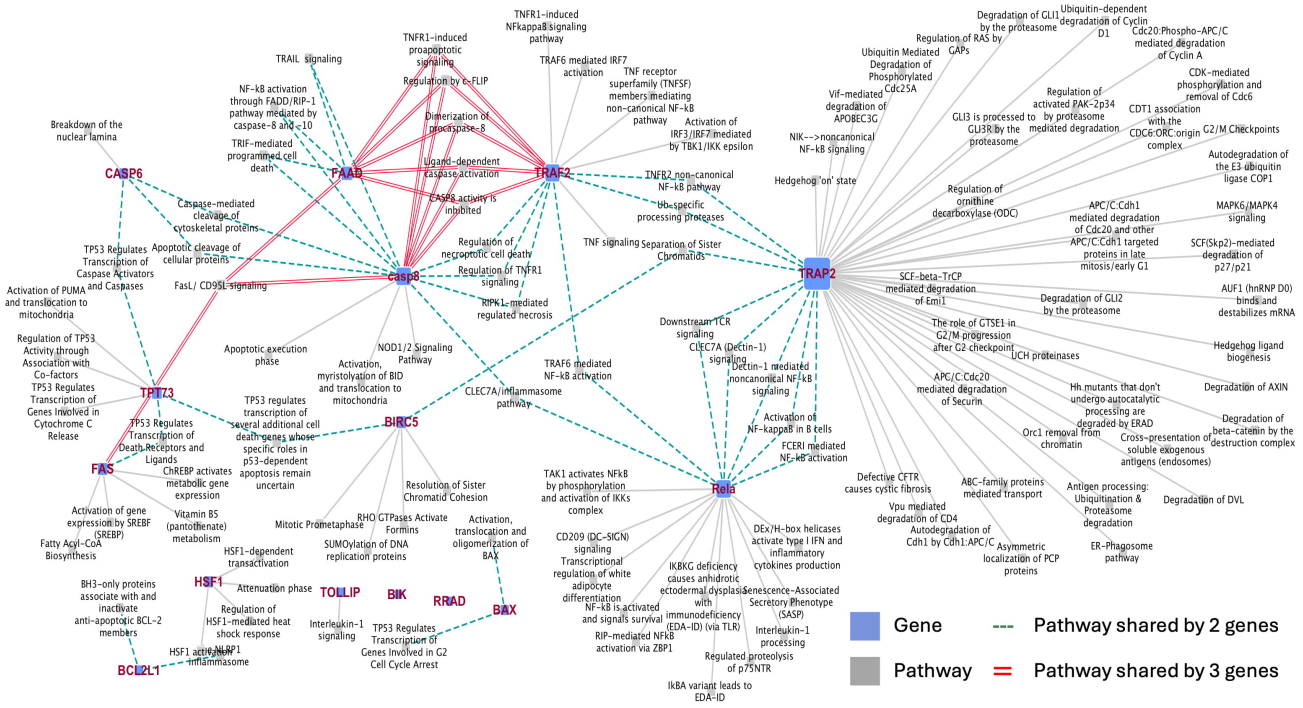

Fig. 1. Interaction network maps of 15 hub genes and their crosstalk among the pathways. The hub genes are represented as squared nodes (blue). The node size grows in relation to their "connectedness" according to the number of pathways they interact with. The grey lines represent those pathways exclusively related to one of the 15 selected genes. The dotted cyan lines connect the pathways shared by two genes. The double red lines connect pathways shared by at least three genes.

MAPKs, and *NFKBs*. These genes were found to be highly down-regulated in WERI-Rb-1 cells after DAC treatment. Additionally, 24 genes that act as positive regulators of DNA damage and repair signaling, including *PARP1* and *LIG4*, were up-regulated in the surviving WERI-Rb-1 cells after 96 h of DAC treatment. Interestingly, in the cone photoreceptor lineages of primary tumors, the top up-regulated genes (Log FC $\geq$4) included those playing a key role in tumor progression, such as *BIRC5* oncogene. We found these genes highly down-regulated at early time points in WERI-Rb-1 cells following DAC treatment. Among the 282 down-regulated genes in primary tumors, more than 200 are associated with cell cycle arrest and pro-apoptotic signals, such as *FAS*, *BIK*, *CASP8*, and *CASP6*. Additionally, 27 of these genes are functionally related to retina development, visual perception, and rhodopsin-mediated signaling pathways. Examples include *PPM1D*, a photoreceptor-related gene, and *AKAP12*, which plays a role in the hemato-retinal barrier [20,21]. These genes were significantly up-regulated in WERI-Rb-1 cells after DAC treatment, suggesting that DAC, as an epigenetic drug, may help restore retinal function by reversing the epigenetic silencing of key factors involved in retina development. A network map of DEGs common to WERI-Rb-1 cells and primary tumors was generated to identify potential hub genes and their crosstalk among pathways. The analysis revealed 15 hubs/driver genes that are tightly interconnected, sharing numerous pathways primarily associated with the regulation of TNF-, FAS-, p53-dependent apoptotic signaling, and NF-κB pro-survival activity (Fig. 1).

In addition, we developed a protein-protein interaction network map that highlights the central role of these 15 hub genes in regulating numerous proteins/factors (**Supplementary Fig. 2**). Notably, the oncogenes *TRAF2*, *RELA*, and *BIRC5*, which play pivotal pro-survival roles and exhibit numerous interactions with their neighboring proteins, are highly up-regulated in primary tumors but down-regulated early after DAC treatment. Conversely, *FAS* and *CASP8*, which are involved in regulating extrinsic apoptosis pathways, along with *BAX*, *BCL2L1*, *HSF*, and *CASP6*, key players in intrinsic apoptosis, are highly up-regulated in DAC-treated WERI-Rb-1 cells and are expressed at lower levels in primary tumors. These genes exhibit numerous interactions with proteins/factors that regulate cell fate. Since bulk RNA-seq studies are primarily designed to provide general transcriptomic data for entire tissue samples, they inherently do not capture the tumor heterogeneity of Rb [34]. Therefore, single-cell RNA sequencing (scRNA-seq) analysis was applied to verify the central role of the 15 hub/DAC-driven genes in the genesis and malignant progression of retinoblastoma. Two publicly available single-cell transcriptome datasets [23,24], comprising human normal retina cells (organoids and retinospheres) and patient-derived sporadic

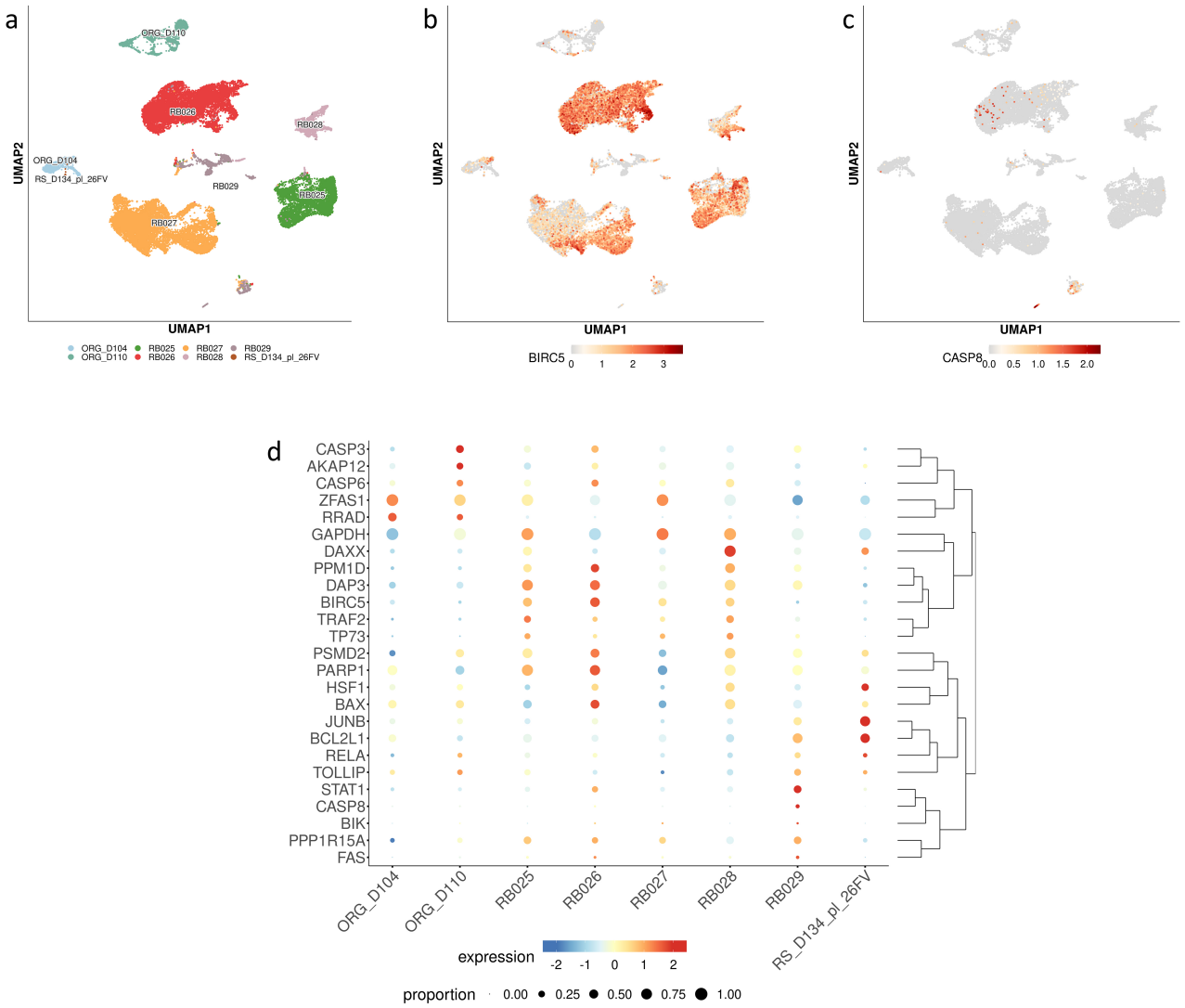

Fig. 2. Single cells expression profiles of DEGs including the 15 key/hub genes in selected normal and primary tumor samples. (a) Selected patient's derived retinoblastoma samples (RB025; RB026; RB027; RB028; RB029), human normal retina organoids (ORG_D104; ORG_D110) and single cell fetal retina (RS_D134_pl_26FV). Representative gene expression of selected genes: (b) restricted clusters (cells cut SCT_snn_res.0.35) for *BIRC5* gene expression and (c) restricted clusters (cells cut SCT_snn_res.0.35) for *CASP8* gene expression. (d) Bubble plot showing expression of several genes (listed in Table 1) in patient-derived retinoblastoma and normal retinal single-cell RNA-seq. The radium of the bubble indicates the prevalence of expression, the color represents the log of up and down expression in any of the sample datasets. DEGs, differentially expressed genes.

retinoblastoma cells of different intraocular retinoblastoma classification (IIRC) were analyzed (**Supplementary Table 1**). Comparative computational analysis at the single-cell level identified 25 subclusters annotated with highly expressed genes (see https://ankushs.shinyapps.io/Retinoblastoma_GSE196420/). For each set of normal cells (ORG_D104; ORG_D1110; and RS_D134_pl_26FV) and primary retinoblastoma cells (RB025; RB026; RB027; RB028; RB029) (Fig. 2a) we describe the expression profiles of DEGs, including the 15 hub genes. UMAP images in Fig. 2b,c illustrate the expression of two representative genes, namely *BIRC5* and *CASP8*.

Most of the key genes found to be up- or down-regulated in WERI-Rb-1 after DAC treatment, as listed in Table 1, show an inverse correlation in expression compared to those identified in subclusters of patient-derived single-cells (Fig. 2d). Among the 15 hub genes shown in Fig. 1, the *BIRC5* and *TRAF2* genes, are mostly overexpressed in primary tumor cells (RB025, RB026, RB027, RB028) and are highly down-regulated in DAC-treated WERI-Rb-1 cells. Similarly, *DAXX* and *HSF1*, which are down-regulated after DAC treatment, are primarily overexpressed in primary tumors (e.g., RB028) and in fetal retinas (RS-D134_lp_26FV). Meanwhile, the regulation of *PPP1R15A*, *RRAD*, *FAS*, *CASP6*, *CASP3*, *BAX*,

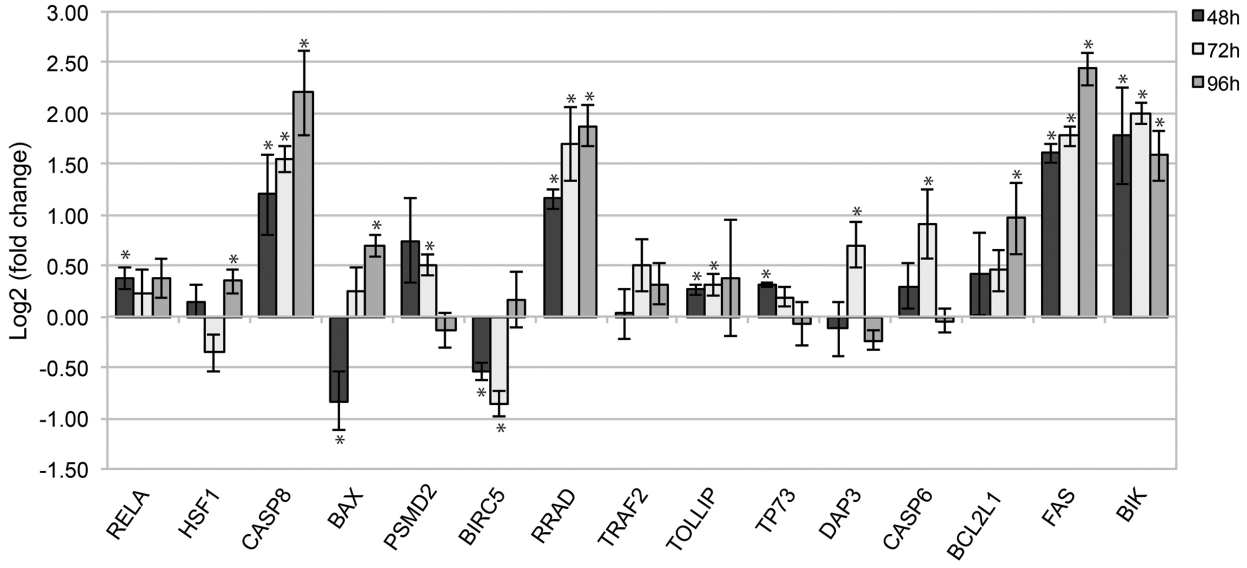

Fig. 3. Gene expression analysis by qPCR of WERI-Rb-1 cells treated with DAC. The histogram shows the relative expression of target genes in DAC-treated WERI-Rb-1 samples, compared to the control untreated samples, after 48, 72, and 96 h of treatment. Data were analyzed using the comparative cycle threshold method ($\Delta\Delta$CT), where β-actin was used as a housekeeping gene and untreated samples as normalizer. Results are shown as $\log_2$ fold change values so that the x-axis (y = 0) represents values for controls ($\log_2$ fold change of controls = 0; above 0 means up-regulated; below 0 means down-regulated). Data are reported as mean ± SD values (*t*-test **p* < 0.05).

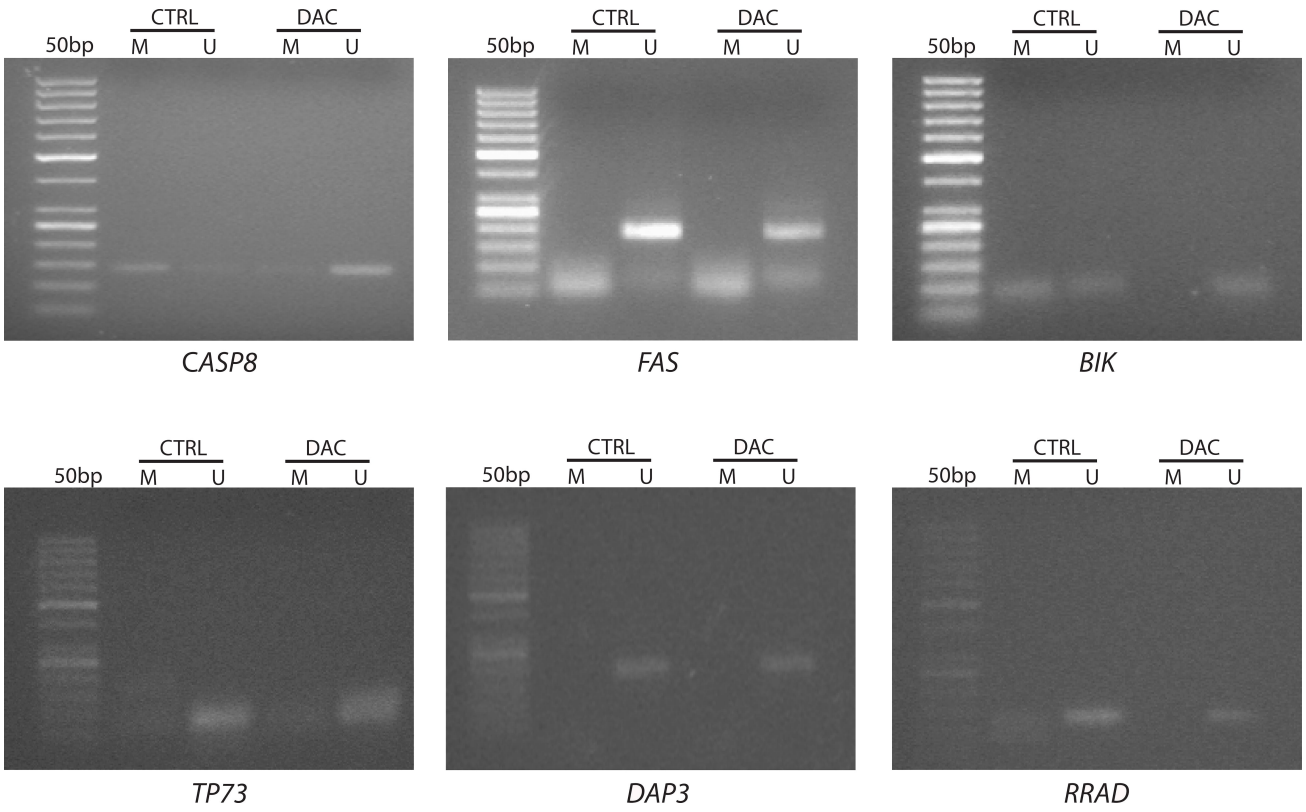

Fig. 4. Agarose gels displaying the promoter's methylation status of selected genes in WERI-Rb-1 samples. Representative Methylation-Specific PCR images show amplified products in untreated (CTRL) and DAC-treated (DAC) samples using specific primer pairs for methylated (M) and unmethylated (U) DNA. The gel images show the presence of a methylated band for *CASP8* and *BIK* genes in untreated WERI-Rb-1 cells (CTRL), indicating promoters' methylation in this retinoblastoma cell line.

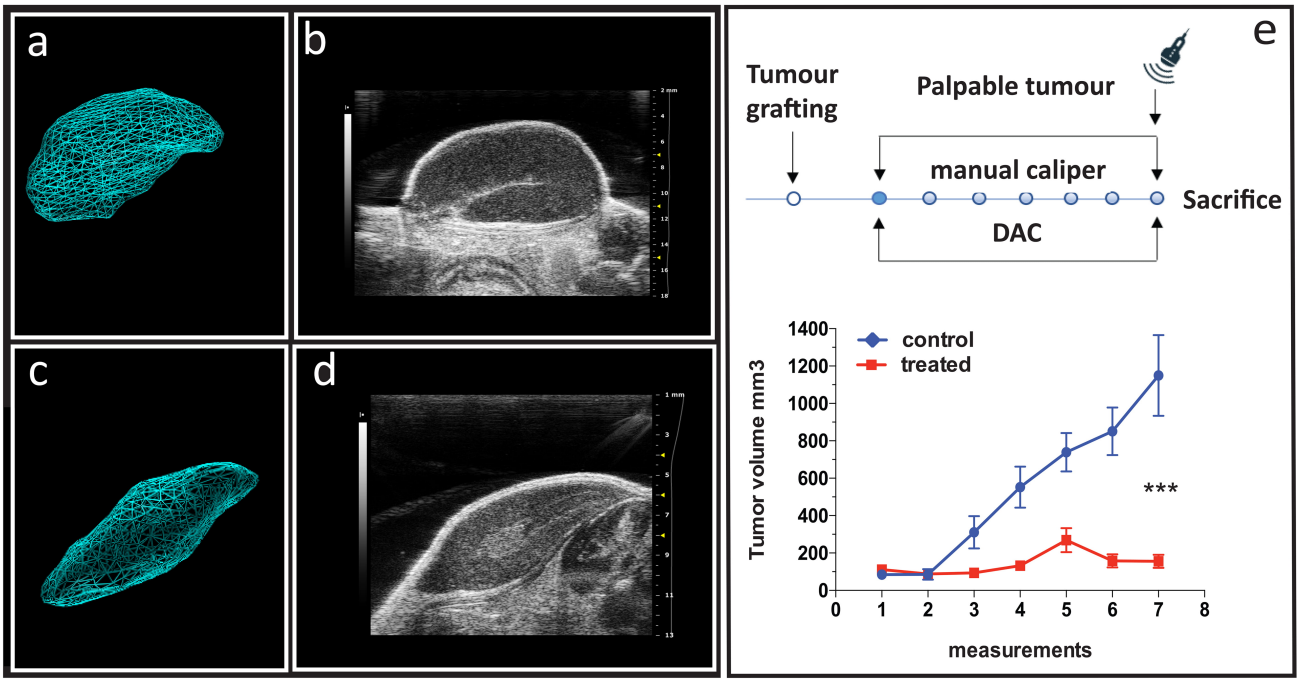

Fig. 5. The effect of DAC treatment on cancer growth in WERI-Rb-1 xenografts. (a) Representative images of echo-graphic acquisition and (b) 3D reconstruction images of control xenograft tumors (n = 7). (c) Representative images of echo-graphic acquisition and (d) 3D reconstruction images of treated xenograft tumors (n = 7). Images were collected during the last *in vivo* confirmatory session of echo-graphic acquisition using the VEVO 2100 imaging system (frame acquisition by length, 0.11 mm frame step for 3D reconstruction measurement). (e) Top panel: experimental protocol sketch with dots representing sections of manual caliper measurements and DAC treatment injections; bottom panel: tumor growth curve in control (blue line) and treated (red line) experimental groups. Volumes (mm^3) were collected bi-weekly by manual caliper throughout the experiment and expressed as mean values ± SEM. ***$p < 0.001$ (TW-ANOVA RM).

CASP8, and *BIK* genes, mainly involved in cell growth arrest and apoptotic signaling and significantly overexpressed in DAC-treated WERI-Rb-1 cells, are expressed at low levels in organoids (ORG_D104 and ORG_D110) and in all primary tumor samples (RB025, RB026, RB027, RB028, and RB029) (Fig. 2d). The overall data suggest that the epigenetic alterations may be involved in tumor progression and that the identified 15 hub/driver genes could serve as key targets for DAC treatment in primary retinoblastoma tumors.

3.2 Validation of the 15 Hub Genes Expression by qPCR Analysis

To test the robustness of the computational data analysis, quantitative PCR was performed on the selected set of 15 hub/driver genes, which showed high differential expression in WERI-Rb-1 cells after DAC epigenetic treatment (Fig. 3).

We noted a significant up-regulation of several pro-apoptotic genes, namely *FAS*, *CASP8*, *BIK*, and the tumor suppressor gene *RRAD*, at all time-points analyzed ($p < 0.05$ at 48, 72, and 96 h). Gene expression changes were observed for other pro-apoptotic genes only at certain time points, such as *HSF1* ($p < 0.05$ at 72 h), and *DAP3*, *TP73*, *PSMD2*, and *CASP6* ($p < 0.05$ at 48 and 72 h). It is also noteworthy that other genes, such as *BAX* and *BCL2L1*, which encode apoptotic activators that regulate mitochondria membrane potential, were significantly overexpressed only at the latest time point ($p < 0.05$ at 96 h). On the other hand, the *BIRC5* oncogene underwent early significant down-regulation that was maintained over a long period ($p < 0.05$ at 48 and 72 h), suggesting an apoptotic response. Our qPCR analysis of DAC-treated WERI-Rb-1 cells confirmed the overall trend of mRNA expression regulation observed in the previous microarray analysis (Table 1).

3.3 Methylation Status of Selected Hub Genes

To assess the potential effect of DAC on modulating the expression of key genes, we employed Methylation-Specific PCR (MSP) to examine the epigenetic status of selected up-regulated genes, that are commonly epigenetically silenced in tumors. As shown in Fig. 4, changes in DNA methylation patterns in CpG-rich regions of promoters were observed for the *CASP8* and *BIK* genes. For both genes, the promoter methylation levels (M) in untreated samples (CTRL) shifted to unmethylated patterns (U) following DAC treatment. Interestingly, for *BIK*, two bands of

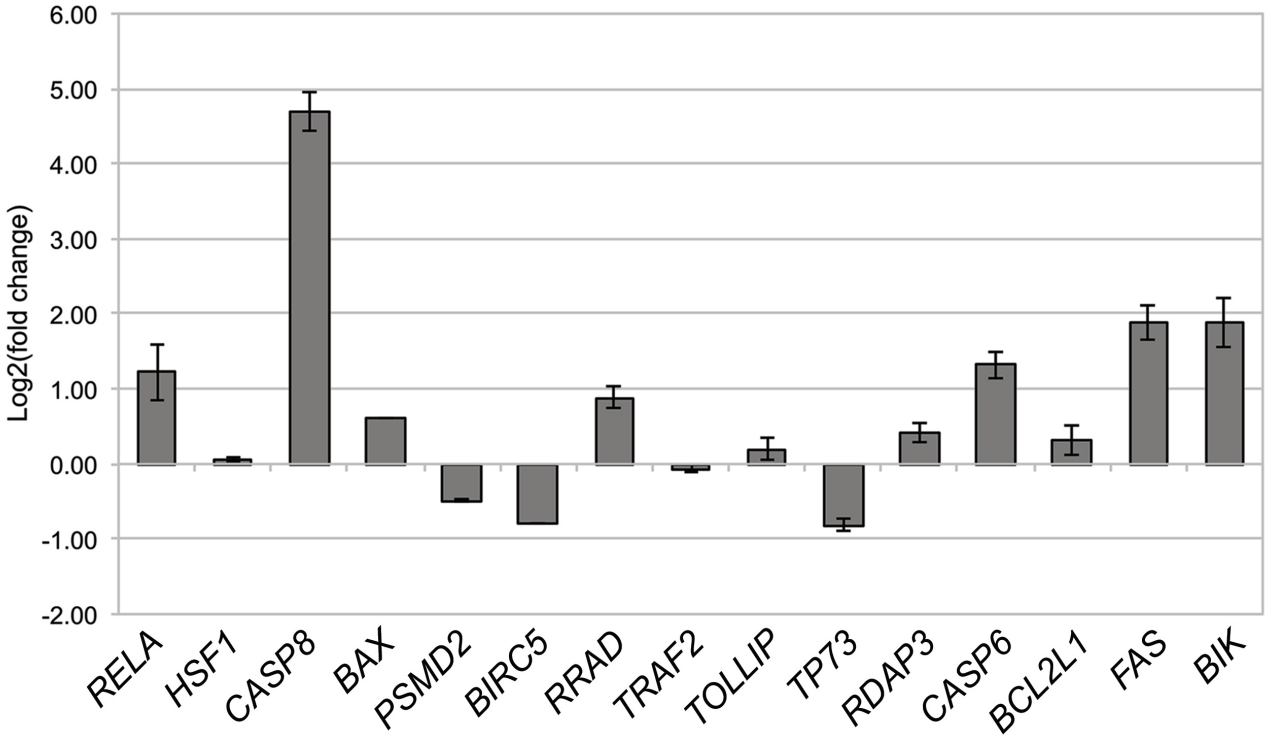

Fig. 6. Gene expression analysis by qPCR of tumor xenografts. The histogram shows the relative expression of target genes in DAC-treated tumor xenograft samples, referred to the control untreated samples. Data were analyzed using the comparative cycle threshold method ($\Delta\Delta$CT), where β-actin was used as a housekeeping gene and untreated tumor xenografts as normalizer. Results are shown as $\log_2$ fold change values so that the x-axis (y = 0) represents values for controls ($\log_2$ fold change of controls = 0; above 0 means up-regulated; below 0 means down-regulated). Data are reported as mean $\pm$ SD values.

similar intensity appeared in the control sample: one corresponding to the methylated pattern and the other to the unmethylated one, indicating the possibility of allele-specific methylation, a common occurrence in tumors. In contrast, the CpG islands of *FAS*, *TP73*, *DAP3*, and *RRAD* gene promoters appeared unmethylated in both control and DAC-treated cells. Overall, these results suggest that DAC modulates gene expression in WERI-Rb-1 cells through a dual mechanism: direct, locus-specific changes in CpG islands methylation, as seen for *CASP8* and *BIK*, and an indirect or nonspecific effect leading to the activation of downstream effectors, without altering cytosines methylation, as previously suggested in the literature [29].

3.4 DAC Inhibits Tumour Progression In Vivo

3.4.1 DAC Antiproliferative Effect in the Rb Xenograft Model

To better mirror the pathology and clinical therapeutic response, we first evaluated the biological anticancer performance of DAC *in vivo*, using a xenograft mouse model (Fig. 5). DAC was administered systemically (i.v.) to WERI-Rb-1 xenografted immunosuppressed mice twice a week for 3 weeks. At the end of the treatment, a significant reduction in the tumor volume was measured in treated (155.90 $\pm$ 32.44 mm^3) mice compared to untreated (1115.01 $\pm$ 215 mm^3) ones. Furthermore, *ex vivo* analysis of expression profiles of 15 hub genes, performed on collected tumor specimens (Fig. 6), was consistent with previous *in vitro* findings (Fig. 3). qPCR data indeed revealed that *FAS*, *CASP8*, and *BIK* genes were highly up-regulated following treatment with the DNA-demethylating drug. These results further confirm the essential role of the apoptosis-inducing *FAS* gene in causing tumor growth arrest *in vivo*, along with the downstream *CASP8* and *BIK* genes, found methylated in untreated WERI-Rb-1 cells (Fig. 4). Moreover, similar to the *in vitro* findings, the expression of the pro-survival gene *BIRC5* was significantly reduced (Fig. 6), confirming that the demethylating agent DAC may exert both direct and indirect regulatory activity, reverting the expression status of retinoblastoma-related genes *in vivo*.

3.4.2 The DAC Antiproliferative Effect in the Intraocular Rb Model

To better recapitulate the features of retinoblastoma tumors, and mimic the native tumor microenvironment, including stromal cell components and local nutrient supply [35], a mono-ocular orthotopic retinoblastoma model was created. The contralateral, non-implanted eyes served as internal controls to rule out systemic treatment effects

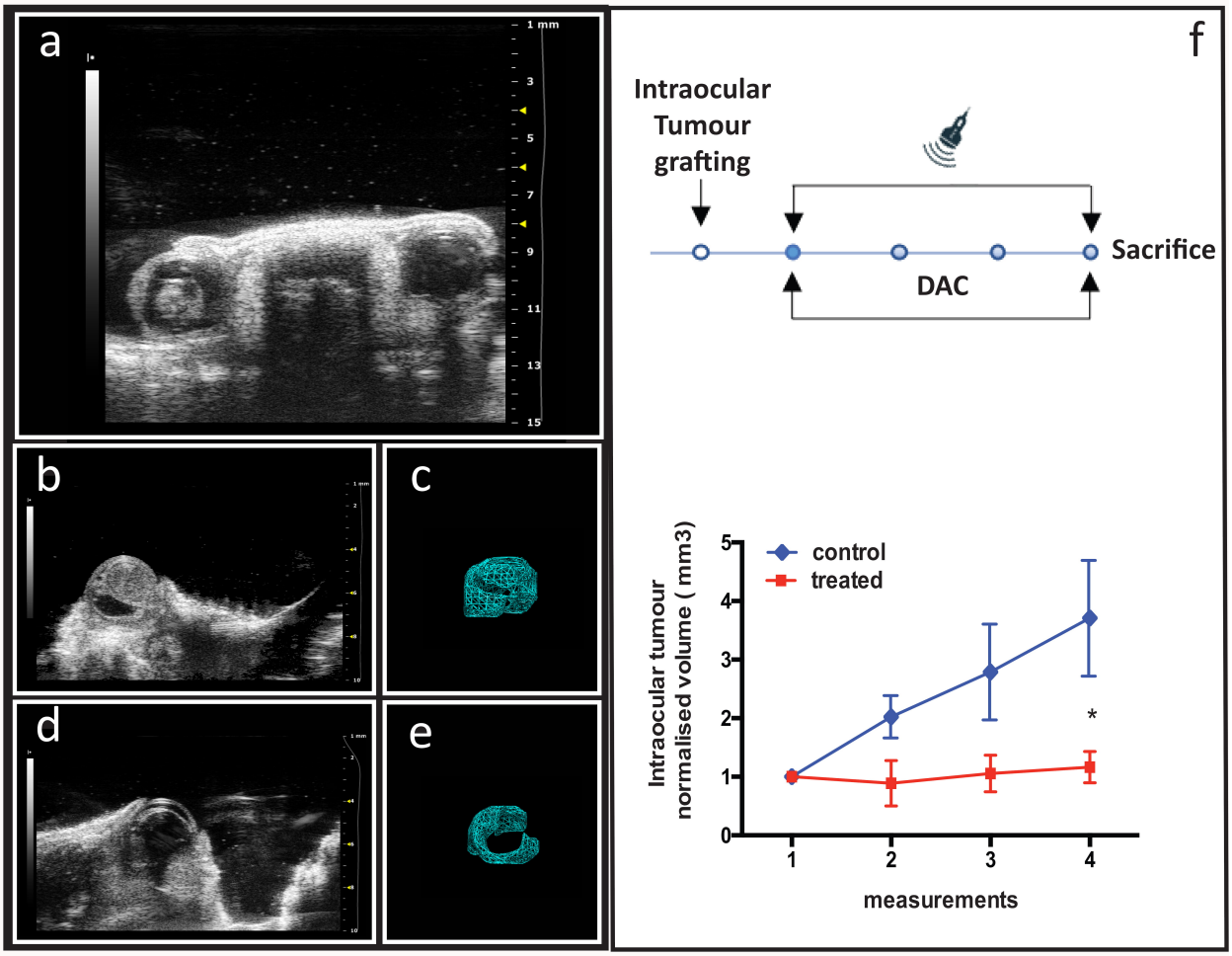

Fig. 7. The effect of systemic DAC treatment on the growth of intraocular retinoblastoma in an orthotopic mouse model. (a) Ocular district of a mono-laterally established model where retinoblastoma tumor mass is growing in the left eye while the right eye is not affected. (b) Representative images of affected eye in control (saline injected) animals (n = 3) and (c) its relative off-line 3D reconstruction used for volume measurement. (d) Representative images of affected eye in treated animals (n = 3) and (e) its relative off-line 3D reconstruction used for volume measurement. (f) Top panel: experimental protocol sketch with dots representing the weekly sections of echo-graphic measurements; bottom panel: tumor growth curve in control (blue line) and treated (red line) experimental groups. Normalized volume values are expressed as mean ± SEM. (TW-ANOVA RM *$p < 0.05$).

(Fig. 7a). Echo-graphic 3D reconstruction imaging of the tumor mass inside the ocular bulb in control (Fig. 7b,c) and treated eyes (Fig. 7d,e) allowed for the longitudinal tumor growth analysis over the three weeks treatment period. We observed reduced tumor growth of intra eye tumor in treated animals (1.16 ± 0.2 mm^3) with respect to controls, which showed a significantly higher tumor volume (3.7 ± 0.9 mm^3) (*$p < 0.05$). These findings demonstrate that systemic DAC reaches the ocular tumor site efficiently and that its gene modulation effect is not hindered by microenvironment-related biological variables (Fig. 7f).

4. Discussion

The study on the genomic and molecular landscape underlying eye cancer development remains a hot topic in the fight against childhood tumors [36–38]. Growing evidence indicates that retinoblastoma arises from epigenetic changes and genetic mutations [3,39] and that reprogramming strategies aimed at restoring the expression of epigenetically silenced genes could serve as promising antitumor therapies [14,38,40–42]. In this regard, there is some evidence that decitabine may have a role in the treatment of Retinoblastoma [10,18]; however, this is the first study correlating DAC treatment effect with the epigenetic restoration of gene expression. Indeed, our *in vivo* preclinical data strongly support this hypothesis. It is known that epigenetic-modifying drugs can alter gene expression by directly or indirectly targeting the epigenetic editors [29]. It has been shown that decitabine operates through a dual mechanism of action. Its incorporation into newly synthesized DNA leads to covalent trapping of the DNA methyltransferase I enzyme and subsequent depletion of

cytosine methylation. However, DAC can also induce a rapid and substantial remodeling of the heterochromatic domains of gene loci enhancing histone acetylation and H3-K4 methylation at unmethylated promoters of oncogenes independently of its effects on cytosine methylation [43]. DAC has previously been used to investigate the impact of promoter hypermethylation effects on human eye development [44]. Here we present a coherent picture in which this demethylating agent modulates the expression of many pro-apoptotic and pro-survival genes together with genes involved in DNA damage and repair signaling by rewriting epigenetic marks in retinoblastoma cells. Furthermore, we demonstrated that the most significant DAC-driven genes may serve as predictive candidate markers for primary retinoblastoma tumors, with 15 key genes acting as hubs or driver genes, conferring a selective advantage to cancer cells.

Notwithstanding the limitations of the preclinical modeling of the flank xenograft, which we emended by using the orthotopic eye tumors, our results show, for the first time, that systemic DAC administration leads to significant tumor growth reduction. Furthermore, our gene expression and methylation analyses indicate that this effect is largely due to the reactivation of pro-apoptotic *CASP8* and *BIK* genes. This re-expression is believed to be the consequence of the direct action of DAC on their promoters' methylation. Conversely for other genes, where no changes in the methylation status of cytosines were observed, an indirect regulatory mechanism of DAC is hypothesized, likely through the alteration of multiple targets in heterochromatin domains such as reversing the silenced histone code at least in the promoter region [43–46]. This could be the case of *FAS*, a pro-apoptotic gene that closely interacts with *CASP8*, and which was found to be overexpressed both *in vitro* and *in vivo* after DAC treatment. Similarly, an indirect regulation can be hypothesized for *BIRC5*, a pro-survival gene found overexpressed in primary tumors but downregulated both *in vitro* and *in vivo* by DAC treatment.

Ultimately, DAC treatment also restored the expression of tissue-specific genes related to photoreceptor function and hemato-retinal barrier development [19,33], further highlighting its potential in treating retina dysfunctions.

Computational analysis of the gene expression profiles after DAC treatment has provided a list of co-regulated gene clusters that may represent potential fingerprints of retinoblastoma phenotype, as well as markers of DAC treatment. In fact, most of these genes have been found as differentially expressed in clusters obtained by the comparative analysis of publicly available datasets of patient-derived tumor samples *vs* normal retina [19,23,24] validating the hypothesis that they may represent markers/candidate drivers of retinoblastoma genesis and progression. Furthermore, the network maps of DEGs highlighted 15 highly interconnected genes that share a high number of pathways and play a pivotal role in regulating numerous proteins/factors. The DAC-induced co-regulated expression of these 15 hubs/driver genes does not seem to be influenced *in vivo* by the complex interplay known to exist between tumor cell-intrinsic, cell-extrinsic, and systemic mediators [47–50]. This evidence suggests that unlike other hypermethylated genes associated with protein signal transduction and external stimulus perception [44], the intracellular reprogramming dynamics of these genes by DAC may be independent from the influence of the tumor microenvironment. In fact, in both subcutaneous and orthotopic xenograft models, our preliminary preclinical data demonstrate a substantial growth arrest in response to DAC treatment. These observations thus lay the foundations for a rational development of effective epigenetic anti-cancer treatments for patients with retinoblastoma.

5. Conclusion

We have described the effects of DAC on the modulation of gene expression encompassing many pro-apoptotic and pro-survival genes, along with genes involved in DNA damage and repair signaling, as well as tissue-specific genes associated with visual signaling in retinoblastoma cells, through rewriting epigenetic marks. Most of the key genes found to be upregulated or downregulated in WERI-Rb-1 cells following DAC treatment exhibit an inverse correlation in expression levels with those identified in primary tumors, highlighting the relevance of the DAC-driven genes as potential actionable markers for primary retinoblastoma tumors. Consistently, DAC induces a significant reduction of tumor growth in *in vivo* retinoblastoma models suggesting that the epigenetic alterations are the essential players in cancer progression and that DAC-driven genes could represent novel key targets of an epigenetic therapy in primary retinoblastoma tumors.

Disclosure

The paper is listed as, "Epigenetic Reprogramming by Decitabine in Retinoblastoma" as a preprint on (Preprints.org) at: https://www.preprints.org/manuscript/202404.1746/v1.

Availability of Data and Materials

The datasets used and/or analyzed during the current study are available from the corresponding authors on reasonable request.

Author Contributions

CC and LG designed the research study. LG, AS, MT, performed the research. LG provided advice on the *in vivo* experiments; MT provided advice of *in vitro* and molecular biology experiments. AS took care of the bioinformatic analysis. CC designed the study and finalised the production of the manuscript. All authors contributed to editorial

changes in the manuscript. All authors read and approved the final manuscript. All authors have participated sufficiently in the work and agreed to be accountable for all aspects of the work.

Ethics Approval and Consent to Participate

All the experiment involving animals were carried out in accordance with EU Directive 2010/63/EU and Italian Ministry of Heath rules and Ethics Committees of the Toscana Life Sciences and the Istituto Superiore di Sanità (ISS) on behalf of Italian Minister of Health (Permit Number: # CNR-030314 and # CNR-101013).

Acknowledgment

We would like to express our gratitude to Dr. Ilaria Naldi and all those who helped us during the writing of this manuscript.

Funding

This research received no external funding.

Conflict of Interest

The authors declare no conflict of interest.

Supplementary Material

Supplementary material associated with this article can be found, in the online version, at https://doi.org/10.31083/FBL33386.

References

[1] Wise J, Hayashi R, Wu T, Malone S, Badawi AA, King A, *et al*. Eye-related quality of life and activities of daily living in pediatric retinoblastoma patients: A single-center, non-controlled, cross-sectional analysis. Pediatric Blood & Cancer. 2023; 70: e30479. https://doi.org/10.1002/pbc.30479.

[2] Dimaras H, Corson TW, Cobrinik D, White A, Zhao J, Munier FL, *et al*. Retinoblastoma. Nature Reviews. Disease Primers. 2015; 1: 15021. https://doi.org/10.1038/nrdp.2015.21.

[3] Tosi GM, Trimarchi C, Macaluso M, La Sala D, Ciccodicola A, Lazzi S, *et al*. Genetic and epigenetic alterations of RB2/p130 tumor suppressor gene in human sporadic retinoblastoma: implications for pathogenesis and therapeutic approach. Oncogene. 2005; 24: 5827–5836. https://doi.org/10.1038/sj.onc.1208630.

[4] Singh U, Malik MA, Goswami S, Shukla S, Kaur J. Epigenetic regulation of human retinoblastoma. Tumour Biology: the Journal of the International Society for Oncodevelopmental Biology and Medicine. 2016; 37: 14427–14441. https://doi.org/10.1007/s13277-016-5308-3.

[5] Poeta L, Drongitis D, Verrillo L, Miano MG. DNA Hypermethylation and Unstable Repeat Diseases: A Paradigm of Transcriptional Silencing to Decipher the Basis of Pathogenic Mechanisms. Genes. 2020; 11: 684. https://doi.org/10.3390/genes11060684.

[6] Costa PMDS, Sales SLA, Pinheiro DP, Pontes LQ, Maranhão SS, Pessoa CDÓ, *et al*. Epigenetic reprogramming in cancer: From diagnosis to treatment. Frontiers in Cell and Developmental Biology. 2023; 11: 1116805. https://doi.org/10.3389/fcell.2023.1116805.

[7] Chianese U, Papulino C, Megchelenbrink W, Tambaro FP, Ciardiello F, Benedetti R, *et al*. Epigenomic machinery regulating pediatric AML: Clonal expansion mechanisms, therapies, and future perspectives. Seminars in Cancer Biology. 2023; 92: 84–101. https://doi.org/10.1016/j.semcancer.2023.03.009.

[8] Katarzyna R, Lucyna B. Epigenetic therapies in patients with solid tumors: Focus on monotherapy with deoxyribonucleic acid methyltransferase inhibitors and histone deacetylase inhibitors. Journal of Cancer Research and Therapeutics. 2019; 15: 961–970. https://doi.org/10.4103/jcrt.JCRT_403_17.

[9] Song YQ, Yang GJ, Ma DL, Wang W, Leung CH. The role and prospect of lysine-specific demethylases in cancer chemoresistance. Medicinal Research Reviews. 2023; 43: 1438–1469. https://doi.org/10.1002/med.21955.

[10] Gherardini L, Sharma A, Capobianco E, Cinti C. Targeting Cancer with Epi-Drugs: A Precision Medicine Perspective. Current Pharmaceutical Biotechnology. 2016; 17: 856–865. https://doi.org/10.2174/1381612822666160527154757.

[11] Li F, Xia Q, Ren L, Nie Y, Ren H, Guo X, *et al*. GSDME Increases Chemotherapeutic Drug Sensitivity by Inducing Pyroptosis in Retinoblastoma Cells. Oxidative Medicine and Cellular Longevity. 2022; 2022: 2371807. https://doi.org/10.1155/2022/2371807.

[12] Salahuddin A, Ghanem H, Omran GA, Helmy MW. Epigenetic restoration and activation of ERβ: an inspiring approach for treatment of triple-negative breast cancer. Medical Oncology (Northwood, London, England). 2022; 39: 150. https://doi.org/10.1007/s12032-022-01765-1.

[13] Zheng Z, Li L, Liu X, Wang D, Tu B, Wang L, *et al*. 5-Aza-2'-deoxycytidine reactivates gene expression via degradation of pRb pocket proteins. FASEB Journal: Official Publication of the Federation of American Societies for Experimental Biology. 2012; 26: 449–459. https://doi.org/10.1096/fj.11-190025.

[14] Greger V, Passarge E, Höpping W, Messmer E, Horsthemke B. Epigenetic changes may contribute to the formation and spontaneous regression of retinoblastoma. Human Genetics. 1989; 83: 155–158. https://doi.org/10.1007/BF00286709.

[15] Karmakar A, Ahamad Khan MM, Kumari N, Devarajan N, Ganesan SK. Identification of Epigenetically Modified Hub Genes and Altered Pathways Associated With Retinoblastoma. Frontiers in Cell and Developmental Biology. 2022; 10: 743224. https://doi.org/10.3389/fcell.2022.743224.

[16] Li HT, Xu L, Weisenberger DJ, Li M, Zhou W, Peng CC, *et al*. Characterizing DNA methylation signatures of retinoblastoma using aqueous humor liquid biopsy. Nature Communications. 2022; 13: 5523. https://doi.org/10.1038/s41467-022-33248-2.

[17] Livide G, Epistolato MC, Amenduni M, Disciglio V, Marozza A, Mencarelli MA, *et al*. Epigenetic and copy number variation analysis in retinoblastoma by MS-MLPA. Pathology Oncology Research: POR. 2012; 18: 703–712. https://doi.org/10.1007/s12253-012-9498-8.

[18] Malusa F, Taranta M, Zaki N, Cinti C, Capobianco E. Time-course gene profiling and networks in demethylated retinoblastoma cell line. Oncotarget. 2015; 6: 23688–23707. https://doi.org/10.18632/oncotarget.4644.

[19] Kooi IE, Mol BM, Moll AC, van der Valk P, de Jong MC, de Graaf P, *et al*. Loss of photoreceptorness and gain of genomic alterations in retinoblastoma reveal tumor progression. EBioMedicine. 2015; 2: 660–670. https://doi.org/10.1016/j.ebiom.2015.06.022.

[20] Davis S, Meltzer PS. GEOquery: a bridge between the Gene Expression Omnibus (GEO) and BioConductor. Bioinformatics (Oxford, England). 2007; 23: 1846–1847. https://doi.org/10.1093/bioinformatics/btm254.

[21] Dennis G, Jr, Sherman BT, Hosack DA, Yang J, Gao W, Lane HC, *et al*. DAVID: Database for Annotation, Visualization, and Integrated Discovery. Genome Biology. 2003; 4: P3.

[22] Maere S, Heymans K, Kuiper M. BiNGO: a Cytoscape plugin to assess overrepresentation of gene ontology categories in biological networks. Bioinformatics (Oxford, England). 2005; 21: 3448–3449. https://doi.org/10.1093/bioinformatics/bti551.

[23] Sridhar A, Hoshino A, Finkbeiner CR, Chitsazan A, Dai L, Haugan AK, *et al*. Single-Cell Transcriptomic Comparison of Human Fetal Retina, hPSC-Derived Retinal Organoids, and Long-Term Retinal Cultures. Cell Reports. 2020; 30: 1644–1659.e4. https://doi.org/10.1016/j.celrep.2020.01.007.

[24] Field MG, Kuznetsoff JN, Zhang MG, Dollar JJ, Durante MA, Sayegh Y, *et al*. RB1 loss triggers dependence on ESRRG in retinoblastoma. Science Advances. 2022; 8: eabm8466. https://doi.org/10.1126/sciadv.abm8466.

[25] Hao Y, Stuart T, Kowalski MH, Choudhary S, Hoffman P, Hartman A, *et al*. Dictionary learning for integrative, multimodal and scalable single-cell analysis. Nature Biotechnology. 2024; 42: 293–304. https://doi.org/10.1038/s41587-023-01767-y.

[26] Sharma A, Akshay A, Rogne M, Eskeland R. ShinyArchR.UiO: user-friendly,integrative and open-source tool for visualization of single-cell ATAC-seq data using ArchR. Bioinformatics (Oxford, England). 2022; 38: 834–836. https://doi.org/10.1093/bioinformatics/btab680.

[27] Ouyang JF, Kamaraj US, Cao EY, Rackham OJL. ShinyCell: simple and sharable visualization of single-cell gene expression data. Bioinformatics (Oxford, England). 2021; 37: 3374–3376. https://doi.org/10.1093/bioinformatics/btab209.

[28] de Groote ML, Verschure PJ, Rots MG. Epigenetic Editing: targeted rewriting of epigenetic marks to modulate expression of selected target genes. Nucleic Acids Research. 2012; 40: 10596–10613. https://doi.org/10.1093/nar/gks863.

[29] Milošević D, Medeiros AS, Stojković Piperac M, Cvijanović D, Soininen J, Milosavljević A, *et al*. The application of Uniform Manifold Approximation and Projection (UMAP) for unconstrained ordination and classification of biological indicators in aquatic ecology. The Science of the Total Environment. 2022; 815: 152365. https://doi.org/10.1016/j.scitotenv.2021.152365.

[30] Langfelder P, Horvath S. WGCNA: an R package for weighted correlation network analysis. BMC Bioinformatics. 2008; 9: 559. https://doi.org/10.1186/1471-2105-9-559.

[31] Zhang B, Horvath S. A general framework for weighted gene co-expression network analysis. Statistical Applications in Genetics and Molecular Biology. 2005; 4: Article17. https://doi.org/10.2202/1544-6115.1128.

[32] Percie du Sert N, Hurst V, Ahluwalia A, Alam S, Avey MT, Baker M, *et al*. The ARRIVE guidelines 2.0: Updated guidelines for reporting animal research. PLoS Biology. 2020; 18: e3000410. https://doi.org/10.1371/journal.pbio.3000410.

[33] Choi YK, Kim JH, Kim WJ, Lee HY, Park JA, Lee SW, *et al*. AKAP12 regulates human blood-retinal barrier formation by downregulation of hypoxia-inducible factor-1alpha. The Journal of Neuroscience: the Official Journal of the Society for Neuroscience. 2007; 27: 4472–4481. https://doi.org/10.1523/JNEUROSCI.5368-06.2007.

[34] Yang J, Li Y, Han Y, Feng Y, Zhou M, Zong C, *et al*. Single-cell transcriptome profiling reveals intratumoural heterogeneity and malignant progression in retinoblastoma. Cell Death & Disease. 2021; 12: 1100. https://doi.org/10.1038/s41419-021-04390-4.

[35] Zhang W, Fan W, Rachagani S, Zhou Z, Lele SM, Batra SK, *et al*. Comparative Study of Subcutaneous and Orthotopic Mouse Models of Prostate Cancer: Vascular Perfusion, Vasculature Density, Hypoxic Burden and BB2r-Targeting Efficacy. Scientific Reports. 2019; 9: 11117. https://doi.org/10.1038/s41598-019-47308-z.

[36] Al-Ghazzawi K, Wessolly M, Dalbah S, Ketteler P, Kiefer T, Bechrakis N, *et al*. PDGF, NGF, and EGF as main contributors to tumorigenesis in high-risk retinoblastoma. Frontiers in Oncology. 2023; 13: 1144951. https://doi.org/10.3389/fonc.2023.1144951.

[37] Hazazi A, AlShehah AA, Khan FR, Hakami MA, Almarshadi F, Abalkhail A, *et al*. From diagnosis to therapy: The transformative role of lncRNAs in eye cancer management. Pathology, Research and Practice. 2024; 254: 155081. https://doi.org/10.1016/j.prp.2023.155081.

[38] Rathore S, Verma A, Ratna R, Marwa N, Ghiya Y, Honavar SG, *et al*. Retinoblastoma: A review of the molecular basis of tumor development and its clinical correlation in shaping future targeted treatment strategies. Indian Journal of Ophthalmology. 2023; 71: 2662–2676. https://doi.org/10.4103/IJO.IJO_3172_22.

[39] Zhang X, Jiang Y, Cai Y, Fu Q, Chen Y. Epigenetics research in eye diseases: a bibliometric analysis from 2000 to 2023. Clinical & Experimental Optometry. 2024; 107: 649–656. https://doi.org/10.1080/08164622.2023.2261929.

[40] Feinberg AP, Koldobskiy MA, Göndör A. Epigenetic modulators, modifiers and mediators in cancer aetiology and progression. Nature Reviews. Genetics. 2016; 17: 284–299. https://doi.org/10.1038/nrg.2016.13.

[41] Jiang Y, Zheng G, Sun X. PRMT5 promotes retinoblastoma development. Human Cell. 2023; 36: 329–341. https://doi.org/10.1007/s13577-022-00807-0.

[42] Kulis M, Esteller M. DNA methylation and cancer. Advances in Genetics. 2010; 70: 27–56. https://doi.org/10.1016/B978-0-12-380866-0.60002-2.

[43] Nguyen CT, Weisenberger DJ, Velicescu M, Gonzales FA, Lin JCY, Liang G, *et al*. Histone H3-lysine 9 methylation is associated with aberrant gene silencing in cancer cells and is rapidly reversed by 5-aza-2'-deoxycytidine. Cancer Research. 2002; 62: 6456–6461.

[44] Berdasco M, Gómez A, Rubio MJ, Català-Mora J, Zanón-Moreno V, Lopez M, *et al*. DNA Methylomes Reveal Biological Networks Involved in Human Eye Development, Functions and Associated Disorders. Scientific Reports. 2017; 7: 11762. https://doi.org/10.1038/s41598-017-12084-1.

[45] Jabbour E, Issa JP, Garcia-Manero G, Kantarjian H. Evolution of decitabine development: accomplishments, ongoing investigations, and future strategies. Cancer. 2008; 112: 2341–2351. https://doi.org/10.1002/cncr.23463.

[46] Yang D, Torres CM, Bardhan K, Zimmerman M, McGaha TL, Liu K. Decitabine and vorinostat cooperate to sensitize colon carcinoma cells to Fas ligand-induced apoptosis in vitro and tumor suppression in vivo. Journal of Immunology (Baltimore, Md.: 1950). 2012; 188: 4441–4449. https://doi.org/10.4049/jimmunol.1103035.

[47] Almet AA, Cang Z, Jin S, Nie Q. The landscape of cell-cell communication through single-cell transcriptomics. Current Opinion in Systems Biology. 2021; 26: 12–23. https://doi.org/10.1016/j.coisb.2021.03.007.

[48] Armingol E, Officer A, Harismendy O, Lewis NE. Deciphering cell-cell interactions and communication from gene expression. Nature Reviews. Genetics. 2021; 22: 71–88. https://doi.org/10.1038/s41576-020-00292-x.

[49] Arnol D, Schapiro D, Bodenmiller B, Saez-Rodriguez J, Stegle O. Modeling Cell-Cell Interactions from Spatial Molecular Data with Spatial Variance Component Analysis. Cell Reports. 2019; 29: 202–211.e6. https://doi.org/10.1016/j.celrep.2019.08.077.

[50] Kolesnikov AV, Luu J, Jin H, Palczewski K, Kefalov VJ. Deletion of Protein Phosphatase 2A Accelerates Retinal Degeneration in GRK1- and Arr1-Deficient Mice. Investigative Ophthalmology & Visual Science. 2022; 63: 18. https://doi.org/10.1167/iovs.63.8.18.